

# MetaPatch: Wireless Sensing for Glucose and Beyond Using Metasurfaces

## ABSTRACT

We propose a novel wireless sensing method, called MetaPatch, for measuring liquid properties, such as glucose or salt concentration, using minimal liquid volume (*e.g.*, inside a 3 mm wide bionic blood vessel). This represents an important step towards applying it to healthcare scenarios. Our approach involves developing a low-cost passive metasurface optimized for maximum reflection frequency response differences across concentrations. To achieve this, we utilize the Cole-Cole model and ABCD transmission matrix to establish an equivalent circuit model for metasurface-based liquid sensing. We optimize the patterns of the metal layer in the metasurface by maximizing the difference in reflected signal's frequency response under varying concentrations. We then utilize HFSS simulation software to fine-tune the metasurface design to account for coupling between multiple metal layers. Our metasurface can be fabricated using paper and aluminum foil at a near-zero cost. Through real-world testbed experiments, we confirm that our optimized metasurface provides approximately a 0.8 MHz frequency shift per 100 mg/dL change in glucose concentration. By fitting a linear relationship between resonance point and concentration, we can achieve a concentration identification error of 28 mg/dL and 81% accuracy for classifying five glucose level categories. Moreover, our method also accurately detects salt concentrations in wound healing saline with a 24 mg/dL tracking error, showing its versatility.

## 1 INTRODUCTION

Diabetes is a major chronic disease that greatly affects society, economy, and patients' quality of life [1]. Continuous glucose monitoring is vital for diabetics, as it helps users understand their condition, prevent hypoglycemic or hyperglycemic events, and assess medication effectiveness [6, 8, 37]. Common glucose monitoring techniques use electrochemical methods, converting glucose concentration into electrical signals for measurement [50]. However, this approach requires invasive procedures like finger-pricks, causing pain, inconvenience, and possible infection, limiting monitoring frequency and range [41]. Thus, a non-invasive, user-friendly, and low-cost glucose monitoring technology could significantly improve the lives of millions of diabetic patients.

Noninvasive glucose monitoring primarily involves infrared spectrum-related techniques and dielectric spectrum-related techniques. Infrared approaches work on the principle that glucose molecules absorb spectra at specific frequencies due

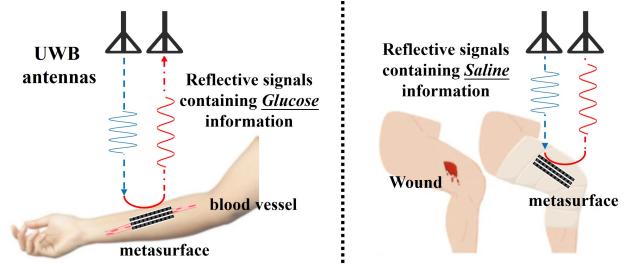


**Figure 1: Metasurface-based glucose sensing and beyond.** This illustration highlights two key examples: (1) Glucose level monitoring for diabetes management, and (2) Wound healing saline monitoring for effective healing

to vibration and rotation [59]. Relevant research and products measure blood glucose by transmitting a laser into subcutaneous tissue and analyzing capillary spectrum [11, 38]. Some researchers use ultrasound and photoacoustic techniques to calculate glucose concentration based on pressure waves and ultrasonic signals generated by glucose molecules' thermal expansion when absorbing the infrared spectrum [11, 38]. Though infrared approaches are viable and have commercial applications, reducing cost and improving laser transceiver integration remain challenging. For example, the Apple Watch has delayed its laser-based glucose measurement feature's release [35, 52].

Dielectric spectrum-based methods leverage changes in dielectric constant due to glucose concentration, and have greater potential. These techniques estimate blood glucose concentration by analyzing electromagnetic (EM) signal propagation characteristics (*e.g.*, attenuation, phase changes) [23]. Compared to infrared spectrum, dielectric spectrum can be obtained using existing radio frequency (RF) resources (*e.g.*, WiFi, UWB, mmWave), available in wearable and mobile devices, enabling low-cost and easy deployment.

Several works estimate liquid concentrations [13, 51] by measuring wireless signal attenuation as they pass through the liquid. This allows inferring its dielectric constant (a.k.a, complex permittivity) [57] and identifying the concentration. However, these methods have limitations for the healthcare scenarios: (1) *Thick liquid samples requirement*: Accurate attenuation factor measurements depend on liquid thickness and equipment sensitivity, and existing work requires substantial liquid thickness (*e.g.*, 10 cm). (2) *Severe multi-path interference*: Existing studies typically use containers with significant surface areas to ensure most EM waves pass through the liquid. However, blood vessels are thin and delicate, making it

challenging to ensure most signals pass through the vessels instead of the nearby tissues.

In this paper, we present a novel glucose sensing system, MetaPatch, by optimizing a passive metasurface sensitive to sense the glucose concentration. Different from existing works, we use reflection EM-spectrum for glucose level measurement, as it enables sensing blood vessels in the wrist, a convenient location for continuous monitoring (e.g., using smartwatches). As shown in Fig. 1, we introduce a metasurface attached to the front of the blood vessels to ensure reflected EM waves contain blood glucose concentration information. Our designed metasurface should couple with blood, and its reflection frequency response ( $S_{11}$  parameters) changes deterministically with blood glucose concentration. Considering the limited sensitivity of commercial RF devices and thin blood vessels, it is necessary to optimize the metasurface design to amplify the change in magnitude-frequency response caused by glucose level changes. To support optimization, we develop an equivalent circuit model to capture the metasurface's coupling with blood (*i.e.*, glucose solutions) and derive reflection coefficients across frequency bands. We search for the impedance of each metal layer in the metasurface by maximizing the difference in reflection coefficients ( $S_{11}$ ) under various glucose concentrations. Since the equivalent circuit model cannot capture near-field coupling between multiple metal layers in a metasurface, we use high-frequency structure simulator (HFSS) [2] to fine-tune the metasurface design and compensate for near-field coupling. Finally we derive a compact geometric pattern of each metasurface layer based on the obtained impedance value. Each element is less than one-tenth of the wavelength of the operating frequencies. The final metasurface achieves desirable resonance frequency point shifts associated with changes in liquid concentration when attached to the solutions inside different containers.

We fabricate our optimized metasurface design using A4 paper and aluminum foil for the metal layers, and PVC board for the substrates at close to 0 cost. We perform extensive experiments to demonstrate the effectiveness of our proposed MetaPatch for liquid concentration sensing. We construct containers with 3 mm thickness and bionic arm model simulating human blood vessels, and utilize a glucose solution as a substitute for blood [9, 56] and precisely control the glucose concentration to obtain ground truth for quantitative analysis. Experimental results show our metasurface successfully couples with the glucose solution and produces resonance frequencies. With directional UWB antennas and vector network analyzer, our optimized metasurface achieves a 0.8 MHz frequency shift per 100 mg/dL glucose change. Fitting a linear relationship between resonance point and concentration yields a 28 mg/dL identification error and 81% accuracy in classifying five glucose level categories. The average glucose level identification error ranges from -13.23% to 11.86%, within

the ISO 15197:2013 ( $\pm 15\%$ ) range [25]. Additionally, our method accurately senses wound healing saline [5], including the saline concentration (error of only 24 mg/dL) and volume of the healing water. This facilitates practitioners to monitor the patient's wound healing rate and serves as a reminder to change the gauze.

We conclude by summarizing our contributions:

- We have developed a novel method called MetaPatch for liquid concentration sensing using optimized metasurface design. Our approach involves determining the reflection frequency response based on an equivalent circuit model corresponding to the liquid measurement setup, and identifying a optimal metasurface design that maximizes the difference in  $S_{11}$  parameters across liquid concentrations.
- We develop a compact metasurface unit of only wavelength/10 large. The entire metasurfaces is only  $1.8\text{cm} \times 6\text{cm}$  large and can be attached alongside the blood vessels. It is  $3\text{cm} \times 3\text{cm}$  for sensing wound saline. We demonstrate that it can be fabricated with paper, aluminum foil, and PVC sheet at a near-zero cost.
- To the best of our knowledge, we have developed the first metasurface-based noninvasive system for sensing blood glucose concentrations and beyond. We conduct extensive experiments to verify the effectiveness of MetaPatch. The results demonstrate that our approach is accurate, noninvasive, low-cost, and easy to deploy.

## 2 RELATED WORK

We present an overview of blood glucose monitoring technologies, including commercial glucometers and recent research. These methods are categorized as invasive and non-invasive.

### 2.1 Invasive Glucose Monitoring

Invasive blood glucose monitoring methods, such as finger-stick blood sampling [29] and subcutaneous implantation [24], rely on electrochemistry principles to detect blood glucose levels. Most glucometers use oxidase to react with glucose molecules in blood samples, converting glucose concentrations into electrical signals [22]. Continuous glucose monitoring (CGM) products use long-term implanted sensors with oxidase to detect glucose in subcutaneous tissue fluid[40]. NovioSense develops a blood glucose sensor placed in the eyelid, estimating blood glucose by measuring tear glucose [7]. However, a positive correlation between tear and blood glucose is only achieved with abundant tears.

The academic community has extensively researched implantable blood glucose sensors based on electromagnetic (EM) resonance properties [9, 14, 30]. These studies use sensors near human blood vessels to monitor glucose levels through changes in the sensor's EM resonance difference, induced by changes in the equivalent capacitance of blood

glucose concentration [30]. However, these methods require sensor implantation and depend on external wireless communication for data transmission. Despite the effectiveness of invasive glucose monitoring methods, their invasive nature may cause discomfort and high costs, limiting widespread adoption [12, 16].

## 2.2 Non-invasive Glucose Monitoring

Currently, two primary non-invasive blood glucose measurement techniques exist: optical spectroscopy-based methods and EM spectroscopy-based methods.

**2.2.1 Optical spectroscopy based methods.** Optical spectroscopy-based methods operate on the principle that glucose molecules absorb, reflect, and scatter light within specific wavelength ranges. When a light source targets biological tissues, such as blood vessels, the unique spectral signatures can be used to infer glucose concentration [17].

**Near-Infrared (NIR) & Raman shift spectroscopy:** NIR spectroscopy, or absorption spectroscopy, uses wavelengths between 700 and 2500nm to penetrate the skin and interact with glucose molecules[47]. Raman spectroscopy is based on the inelastic scattering of light by molecules, resulting in a wavelength shift of scattered light [27]. A commercial device, CoG, operates on the principle of absorption spectroscopy. It features a light source, real-time color image sensor, and specialized algorithms to assess glucose levels in patients' fingertip capillaries [10].

**Fluorescence spectroscopy:** Fluorescence-based methods use glucose-sensitive fluorescent molecules (fluorophores) that emit light at a specific wavelength when binding to glucose. The emitted light intensity is proportional to glucose concentration, enabling accurate monitoring. Glucosense employs a low-power laser to irradiate nano-engineered quartz glass, causing ions to emit fluorescence in infrared light. The fluorescence signal's degree is then converted to glucose concentration [31, 32].

**Photoacoustic spectroscopy:** The photoacoustic spectroscopy technique works by having glucose molecules absorb light and convert the absorbed energy into heat, causing a local pressure change and generating acoustic waves. This method determines glucose concentration by using an ultrasound transducer to detect the pressure waves and ultrasonic signals produced by thermal expansion when glucose molecules absorb infrared spectra during laser irradiation of blood vessels [4, 44, 52].

Optical spectroscopy-based glucose monitoring faces challenges, including costly, complex laser and spectrometer components, limiting adoption in resource-limited settings. Lag time between glucose changes and detected signals affects real-time monitoring, while signal interference from other

molecules and tissue components complicates accurate glucose measurements.

### 2.2.2 Electromagnetic spectroscopy based methods.

The **EM spectroscopy** method, or dielectric constant spectroscopy, uses high-precision transceivers to detect dielectric constant changes due to blood glucose fluctuations. Analyzing EM wave attenuation enables glucose level estimation. However, existing commercial products only measure attenuation, require fingertip or earlobe measurements, and have a high signal-to-noise ratio, raising costs like GlucoTrack's \$2,120 price [26]. Related studies and techniques, such as liquid classification and concentration recognition, are summarized across various RF bands.

**UWB (Ultra-Wideband):** Ashutosh *et al.* develop LiquID, a low-cost liquid recognition system based on the relationship between the attenuation factor and the dielectric constant, using UWB antennas [13]. However, this method requires multiple experiments with a reference line to measure the decay factor. Moreover, it has not considered measuring dielectric constant in very thin containers. So this method cannot be directly applied to measuring blood glucose levels.

**Wi-Fi:** Fei *et al.* develop LiqRay to sense liquid concentration using attenuation coefficients of multiple frequency points in the Wi-Fi frequency band [51]. However, this method requires a large enough container and is easily affected by multi-path interference, making it unsuitable for blood glucose sensing. Feng *et al.* propose WiMi that uses a learning model to identify liquid with commercial Wi-Fi devices but also requires considerable thickness of liquid [15]. Several studies design wearable EM resonant sensors that are placed close to the arm or lower leg to monitor blood glucose levels [21, 43]. However, since these systems are not passive and require cables to operate, deploying these half-wavelength-size antennas is challenging and not ideal for practical applications.

**RFID:** Unsoo *et al.* propose RF-EATS, a method that involves placing RFID tags on the surface of liquid containers and analyzing the inconsistent spectral features of the reflected signals. A learning-based classifier is designed to determine the authenticity and other characteristics of the liquid [19, 20]. Binbin *et al.* develop a liquid classification system using RFID; however, it is unable to differentiate liquid concentrations at a fine granularity [58]. Since RFID antennas are primarily designed for communication purposes, their response to changes in liquid concentration is not very pronounced, limiting their effectiveness in accurately detecting blood glucose levels.

**mmWave:** Omer *et al.* propose a millimeter-wave (mmWave) remote blood glucose concentration detection system based on the Soli mmWave Radar board [42, 49]. They analyze the reflected signals from specific environments for concentration

classification, making the system very sensitive to the environment. Yumeng *et al.* propose a mmWave liquid sensing system based on a deep learning algorithm and TI mmWave Radar board, which utilizes the reflected signals from liquid containers to classify the liquids [33]. This method requires the collection of a large amount of data, and the material of the liquid container significantly interferes with the reflected waves. Its feasibility in detecting blood glucose concentrations through thin blood vessels has not been validated.

**Terahertz:** Jun *et al.* explore THz and metasurface simulation but lack a system for validation [60]. Some researchers use sub-terahertz radiation (near 0.1 THz) for glucose solution reflectance measurement, showing decreased reflectance with increased glucose concentration, suggesting non-invasive blood glucose measurement potential [53, 55, 60]. However, THz-based sensing faces issues with costly terahertz sources and transceiver antennas, and neither THz nor sub-THz is available on mobile devices.

**Our work:** Our work's unique benefits stem from the careful metasurface design, which allows the reflected EM spectrum to respond to a small change in blood glucose concentration and supports a close-to-zero fabrication.

### 3 METAPATCH DESIGN

#### 3.1 Overview

Permittivity, also known as dielectric constant, is an intrinsic liquid property influenced by its major components. In wireless sensing, permittivity impacts wireless signal transmission and reflection characteristics when interacting with objects. Thus, some studies use reflection or penetration coefficients to estimate permittivity information [13] or identify materials [58]. Minor changes in blood glucose levels cause slight permittivity shifts. Given the blood vessel thickness (*e.g.*, 2-3 mm), these minor permittivity changes result in weak reflectance and penetration changes (*e.g.*, <0.01 dB change for per 100 mg/dL glucose concentration change), which is hard to detect reliably. Hence, a new method is required to accurately measure small permittivity changes to enable accurate concentration sensing.

In this paper, we infer liquid concentration by measuring the reflected EM spectrum information using an optimized passive metasurface attached to the test liquid, enhancing reflected frequency responses due to minor permittivity changes. We first establish an equivalent circuit model to simulate EM wave propagation characteristics when encountering liquids. As the metasurface is equivalent to an LC network, we introduce an additional parallel LC network and optimize its parameters (*i.e.*, metal pattern design) to ensure resonance characteristics – generating resonant coupling at specific frequency points. These resonant frequency points shift as the liquid concentration changes. We use the HFSS simulator

to compensate for coupling between multiple metal layers and fine-tune the metasurface design for target liquid concentration sensing. Therefore, by attaching an optimized metasurface near a container with liquid (*e.g.*, on the skin near blood vessels) and measuring the resonance frequency information of reflected EM waves, we can accurately infer liquid concentration.

In the remainder of this section, we will first introduce the relationship between liquid concentration and permittivity, and provide an in-depth analysis of the equivalent circuit model for metasurface-aided liquid sensing. Then, we will present equivalent circuit based optimization to derive an initial metasurface design. We will refine our metasurface using HFSS simulation to take into account the coupling between multiple metal layers of the metasurface.

#### 3.2 Permittivity versus Liquid Concentration

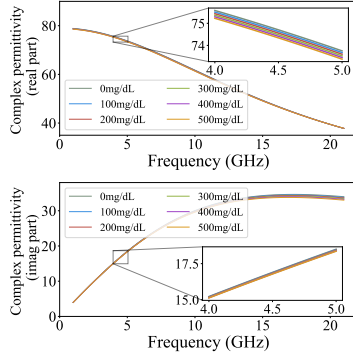
In electromagnetism, absolute permittivity quantifies a material's capacity to store energy from an electric field, influencing its interaction with the field and EM wave propagation. When an EM wave encounters liquid, it undergoes both reflection and transmission, altering the properties of the reflected and transmitted signals (*e.g.*, amplitude and phase) based on the liquid's permittivity. Therefore, characterizing permittivity for different glucose concentrations is a promising step towards enabling accurate sensing.

The permittivity is often represented by the relative permittivity  $\epsilon_r$ . It is the ratio of the absolute permittivity  $\epsilon$  and the vacuum permittivity  $\epsilon_0$ , which can be treated as a complex function of the frequency:  $\epsilon_r(\omega) = \epsilon'_r(\omega) - j\epsilon''_r(\omega)$ , where  $\omega$  is the angular frequency,  $\epsilon'_r$  is the dielectric constant (real part of relative permittivity) representing electric field storage, and  $\epsilon''_r$  is the loss factor (imaginary part) representing energy loss through absorption, conduction, and relaxation [57]. The Cole-Cole model effectively captures frequency-dependent permittivity behavior, which allows us to fit relative permittivity properties using finite measured values at specific frequencies. The model [28] captures complex permittivity as follows:

$$\epsilon_r = \epsilon_\infty + \sum_{i=1}^n \frac{\epsilon_s - \epsilon_\infty}{1 + (j\omega\tau_n)^{1-\alpha_n}} + \frac{\sigma_i}{j\omega\epsilon'_0} \quad (1)$$

where  $\epsilon_s$  and  $\epsilon_\infty$  denote the limits of permittivity at low and high frequencies,  $\epsilon_0$  refers to the permittivity of free space,  $\tau$  is the relaxation time in seconds,  $\alpha$  is the distribution parameter that describes the symmetrical broadening of the relaxation loss peak, and  $\sigma_i$  represents the ionic conductivity. The relaxation function characterizes the loss peak and the decline in  $\epsilon'$  [18].

To obtain the frequency-dependent permittivity model for glucose solutions with varying concentrations, a limited range of permittivity values (real and imaginary parts) are measured


**Figure 2: Complex permittivity**

**of glucose solutions (water back-** **Figure 3: (a)** Experimental setup for measuring the  $S_{11}/S_{21}$  coefficients. **(b)** Equivalent circuit model: liquid is modeled as a transmission line

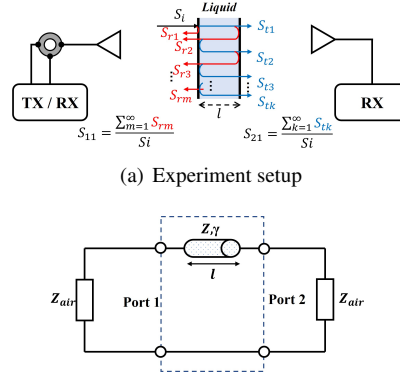
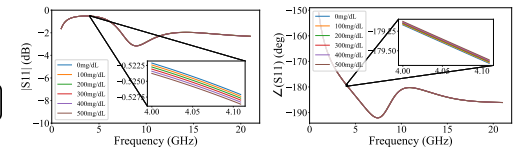
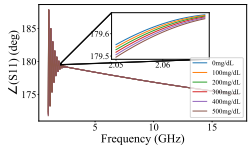
using a liquid probe and a vector network analyzer [56]. These values are used to fit the Cole-Cole model parameters. In this case, a single pole Cole-Cole model ( $n = 1$ ,  $\alpha = 0$ , simplified as a Debye model) is employed to fit the permittivity model for different glucose concentrations, with fitted parameters shown in Table 1. The frequency-dependent complex permittivity for various glucose concentrations is depicted in Fig. 2. Varying concentrations weakly impact permittivity; within the 20 GHz range, as concentration changes from 0 to 500 mg/dL, the real part decreases by approximately 0.4 ( $\approx 0.5\%$ ), while the imaginary part increases by about 0.2 ( $\approx 1\%$ ).

Next, we analyze how permittivity changes affect reflectivity and transmittance of EM waves interacting with glucose solutions across concentrations. The experimental setup is shown in Fig. 3(a). EM waves from the transmitting antenna undergo reflection and transmission behaviors at the interfaces of different materials, depending on permittivity and liquid thickness. The equivalent circuit model is in Fig. 3(b). The liquid is modeled as a transmission line [45], involving three parameters related to the liquid:  $l$ ,  $Z$ , and  $\gamma$ , where  $l$  is liquid thickness,  $Z$  is characteristic complex impedance, and  $\gamma$  is the complex propagation constant. Both  $Z$  and  $\gamma$  can be expressed through relative permittivity as follows:

$$Z = \sqrt{\frac{\mu}{\epsilon}} = \sqrt{\frac{\mu_0 \mu_r}{\epsilon_0 \epsilon_r}} = Z_0 \sqrt{\frac{\mu_r}{\epsilon_r}} \quad (2)$$

$$\gamma = \frac{j\omega \mu}{Z} = \frac{j\omega \mu_0 \sqrt{\mu_r \epsilon_r}}{Z_0} = \gamma_0 \sqrt{\mu_r \epsilon_r}$$

where  $\omega$  is the incident EM signal's angular frequency,  $Z_0$  is free space's characteristic impedance ( $377 \Omega$ ),  $\gamma_0$  is free space's propagation constant ( $\frac{j\omega}{c}$ ), and  $c$  is the speed of light. We set liquid  $\mu_r$  to 1, since glucose solutions are not magnetic materials.


**(b) Equivalent circuit**

**(a) Thickness of the liquid: 3 mm**

**(b) Thickness of the liquid: 10 cm**

**Figure 4: Variations in  $S_{11}$  parameters (reflection attenuation and phase delay) in response to glucose concentration changes across different liquid thicknesses**

Conc. (mg/dL)	0	100	200	300	400	500
$\delta_\epsilon$	69.155	69.034	68.782	68.375	67.901	67.550
$\epsilon_\infty$	9.991	10.028	10.142	10.483	10.956	11.267
$\tau(1e^{-12})$	9.26	9.24	9.22	9.28	9.36	9.42

**Table 1: Parameters of the Cole-Cole models for five different concentrations of glucose solutions**

We can derive the reflection ratio from the equivalent circuit by calculating the ABCD matrix [46]. The ABCD matrix, also known as transmission matrix, is a  $2 \times 2$  matrix used to characterize linear two-port networks' properties in electrical circuits, like ports 1 and 2 in Fig. 3(b). Elements A, B, C, and D can be calculated based on specific components and connections, describing the transmission characteristics (*i.e.*, the relationship between input and output voltage and current). A two-port network with a transmission line circuit can be modeled as the following ABCD matrix:

$$M_{tl} = \begin{bmatrix} A & B \\ C & D \end{bmatrix} = \begin{bmatrix} \cosh yl & Z \sinh yl \\ \sinh yl & \cosh yl \end{bmatrix} \quad (3)$$

The elements of the matrix describe the relationship between input and output voltages and currents along the transmission line. We can then convert the ABCD-parameter to S-parameter to derive the following  $S_{11}$  parameter (*i.e.*, reflection ratio) and  $S_{21}$  parameter (*i.e.*, penetration ratio):

$$S_{11} = \frac{A + B/Z_0 - CZ_0 - D}{A + B/Z_0 + CZ_0 + D} \quad (4)$$

$$S_{21} = \frac{2}{A + B/Z_0 + CZ_0 + D}$$

Fig. 4 shows the  $S_{11}$  curves of EM waves interacting with glucose solutions with varying thicknesses and concentrations over a wide frequency band. From Fig. 4(a), we observe that when the liquid is 3 mm thick, the permittivity change caused by different concentrations has a negligible effect on the  $S_{11}$  parameter in terms of amplitude and phase. The change in

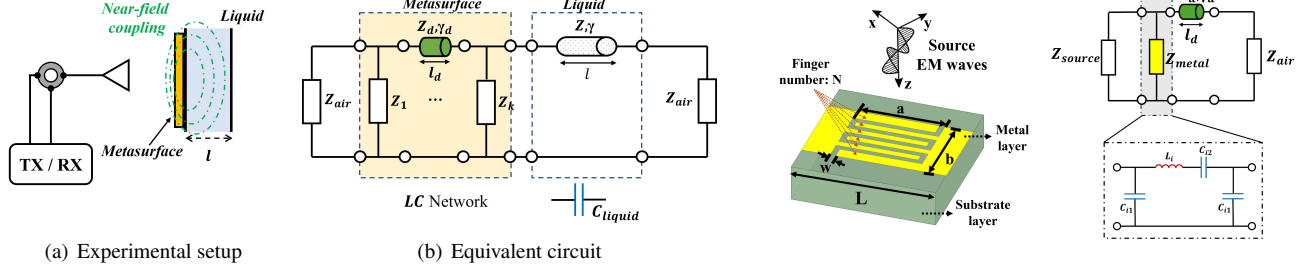


**Figure 5: (a) Experimental setup for measuring the reflection coefficients through a metasurface attached in front of the test liquid. (b) Metasurface can be modelled as an LC circuit network**

$S_{11}$  amplitude is about 0.001 dB, and the phase change is about  $0.01^\circ$  for every 100 mg/dL change. Such variations can easily be overwhelmed by ambient noise. Fig. 4(b) shows the variation of  $S_{11}$  parameters when the liquid thickness is 10 cm. At low frequencies, the  $S_{11}$  parameter oscillates due to the multipath superposition effect of EM waves after multiple reflections and transmissions at the air-liquid interfaces. In this case, the change in  $S_{11}$  amplitude per 100 mg/dL is about 0.001 dB, and the change in phase is about  $0.02^\circ$ . Similarly, the  $S_{21}$  parameters exhibit a subtle change comparable to that of the  $S_{11}$ . In summary, it is nearly impossible to deduce the concentration of glucose solution solely from parameters such as  $S_{11}$  or  $S_{21}$  when the solution's thickness is minimal, *e.g.*, 3 mm, as in blood vessels.

### 3.3 Modeling Metasurface-aided Glucose Sensing

Determining concentration based on a liquid's reflection and transmission of EM waves at various concentrations is challenging when the liquid's thickness is minimal. In the equivalent circuit, the liquid's transmission line is similar to a single capacitor component. A small change in capacitance value can have an insignificant effect on the circuit's behavior. To amplify the impact of subtle capacitance changes due to concentration variations, we draw inspiration from LC resonant circuits. In these circuits, a minor change in capacitance can shift the resonance characteristics, such as the resonance frequency point and the entire frequency response curve. Therefore, our goal is to use metasurfaces for fine-grained liquid concentration sensing, even for liquid with small thicknesses.

The setup of our proposed metasurface-aided liquid concentration sensing system is shown in Fig. 5(a). We place the metasurface in front of the liquid and deduce the liquid concentration by measuring the reflected EM spectrum. The corresponding equivalent circuit is shown in Fig. 5(b), where the incorporated metasurface acts as a complex LC network. Therefore, our objective is to optimize this LC network to best match the liquid capacitance, ensuring that the entire circuit exhibits the high quality resonant characteristics. In

**Figure 6: Left: structure design of an example metasurface unit. Right: equivalent LC circuit of the metasurface**

this manner, the liquid capacitance can maximally alter the resonant characteristic when it experiences a minor change caused by the concentration variations.

Next, we model the LC circuit introduced by the metasurface. As shown in Fig. 6, when the source EM wave propagates along the z-axis and interacts with the metasurface, it first encounters a metal layer. This metal layer is equivalent to a parallel LC circuit in circuit modeling[45]. The LC circuit model is directly related to the metal pattern, which generates an equivalent capacitance (with impedance  $\frac{1}{j\omega C}$ , where  $\omega$  is the angular frequency) and inductance ( $j\omega L$ ) to determine its impedance. Using the metal pattern of Fig. 6 as an example, this is a passive meta-atom design with lumped element planar capacitors and a multi-finger periodic element [3]. Each pair of fingers form capacitors, *i.e.*,  $C_{i1}$  and  $C_{i2}$ , and virtual parasitic inductance caused by the connection of the capacitors, *i.e.*,  $L_i$ . This type of meta-atom design adds an additional LC network to the liquid sensing circuit model. For simplicity, we denote  $Z_{metal}$  as the impedance of the metal layer. The ABCD matrix of a parallel impedance ( $Z$ ) is expressed as:

$$M_{||} = \begin{bmatrix} A & B \\ C & D \end{bmatrix} = \begin{bmatrix} 1 & 0 \\ \frac{1}{Z} & 1 \end{bmatrix} \quad (5)$$

After the EM wave interacts with the metal layer, it penetrates the substrate layer, which is equivalent to a transmission line, just like the liquid modeling. The substrate layer has its own unique properties, such as permittivity and thickness. Similarly, the ABCD matrix of the substrate transmission line can be characterized by Eq. 3 with its propagation constant and characteristic impedance.

To this end, we can build a complete equivalent circuit model for glucose sensing based on metasurface assistance. For an example setup, as shown in Fig. 7, the metasurface consists of four metal and substrate layers, respectively. We construct four parallel impedance components for the meta layers and four transmission line components for the substrate layers. The liquid is in a container with walls modeled as transmission lines. Note that, in Fig. 7, other components are available for various test environments. For instance, if

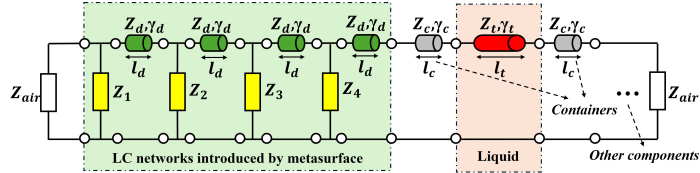


**Figure 7: Equivalent circuit based optimization model of the glucose sensing with a multi-layer metasurface**

measuring the glucose concentration in blood vessels within the arm, container layer 1 represents the skin, while container layer 2 is replaced by other components such as fat, muscle, and bone. A nice property of ABCD matrix theory is that the ABCD matrix of an entire circuit can be derived from the product of ABCD matrices corresponding to individual components. Let  $M_{||}^1, M_{||}^2, M_{||}^3$ , and  $M_{||}^4$  represent the ABCD matrices of the four metal layers in the metasurface,  $M_{tl}^{s1}, M_{tl}^{s2}, M_{tl}^{s3}, M_{tl}^{s4}$ , represent the ABCD matrices of the substrate layers, and  $M_{tl}^{c1}$  and  $M_{tl}^{c2}$  represent the ABCD matrices of the container layers, and  $M_{tl}^g$  represents the ABCD matrix of the glucose solution. Thus, the overall ABCD matrix of the system can be expressed as:

$$\begin{aligned} M_{total} &= M_{||}^1 M_{tl}^{s1} M_{||}^2 M_{tl}^{s2} M_{||}^3 M_{tl}^{s3} M_{||}^4 M_{tl}^{s4} M_{tl}^{c1} M_{tl}^g M_{tl}^{c2} \\ &= \begin{bmatrix} A_{total} & B_{total} \\ C_{total} & D_{total} \end{bmatrix} \end{aligned} \quad (6)$$

By following this approach, we apply Eq. 2 to derive the characteristic impedance  $Z_{glucose}$  and  $\gamma_{glucose}$  from the relative permittivity parameters. Then we can calculate the entire ABCD matrix values and combine with Eq. 4 to obtain the  $S_{11}$  parameters. This  $S_{11}$  parameter represents the reflection frequency response information when the EM waves interact with the metasurface and the glucose solution.

### 3.4 Optimizing Metasurface Design

After obtaining the  $S_{11}$  parameters as a function of glucose concentration, we need to optimize the metasurface design to maximize the  $S_{11}$  parameter differences corresponding to concentration variations. By doing so, we can maximize the sensitivity and accuracy of metasurface-assisted glucose level detection, thereby enabling effective glucose monitoring.

**Optimization Objective.** We set up the liquid sensing environment (*e.g.*, in a container or blood vessel) and various environment parameters, such as container thickness. Next, we determine the liquid thickness (*e.g.*, 3 mm), the number of metal and substrate layers in the metasurface, and each substrate layer's thickness (*e.g.*, 0.3 mm). Then, we set the frequency range for liquid sensing, such as 5.5-6.5 GHz. The user can set the working frequency range, and the optimized metasurface will resonate with the test liquid within that range.

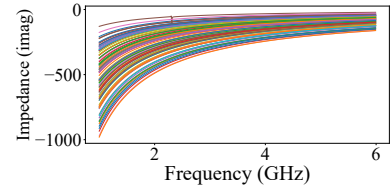


**Figure 8: Impedance vs. frequency plot of the metasurface unit with different geometric parameters**

We recommend concentration sensing in the UWB frequency band (*e.g.*, 1-8 GHz). At higher frequencies (*e.g.*, 20 GHz), glucose solution causes significant EM wave loss (absorption) due to the large imaginary part of the permittivity.

Our goal is to optimize the design of each metal layer so that the  $S_{11}$  parameters are most sensitive to changes in glucose concentration. To simplify the optimization objective, we equate each metal layer to an impedance, where the impedance is a pure complex number, such as  $jX$ . This is because the metal layer can be treated as an ideal electrical conductor. It is worth noting that impedance of the metal layer varies with frequency, so  $X$  here is a function of frequency, *i.e.*,  $X(f)$ . Therefore, our optimization objective is as follows:

$$\max_{X_1(f), \dots, X_k(f)} \sum_{i=1}^m \sum_{j=1, j \neq i}^m ||S_{11}(c_i) - S_{11}(c_j)||^2 \quad (7)$$

where  $X_1(f), \dots, X_k(f)$  represent the impedance functions of the  $k$  metal layers,  $m$  denotes the glucose concentration level number, and  $c_i$  is the  $i$ -th glucose concentration value. For example,  $[c_0, c_1, c_2, \dots, c_5] = [0, 100, 200, \dots, 500]$  mg/dL.  $S_{11}(c_i)$  means the  $S_{11}$  parameters of the glucose solution with concentration  $c_i$ . The optimization goal is to achieve optimal impedance functions maximizing the  $S_{11}$  parameter differences between glucose concentrations. Here, we use the distance between  $S_{11}$  under different concentrations as the optimization target due to its advantages: (1) Maximizing the distances in the frequency response effectively maximizes the sharpness of the resonance frequency (*i.e.*, minimizing  $\min(S_{11})$ ) and the difference in the resonance frequencies (*i.e.*, maximize  $|\text{argmin}(S_{11}(c_i)) - \text{argmin}(S_{11}(c_j))|$ ). (2) Compared to  $\min(\cdot)$  and  $\text{argmin}(\cdot)$  functions, the distance-based loss function has a gradient during backpropagation, which supports gradient descent optimizer.

**Deriving Frequency Dependent Impedance Function.** The metal layer impedance is related to its pattern. In this paper, we use the pattern design shown in Fig. 6 (left part) as our template since it achieves a wide impedance range at a size smaller than a half wavelength. For example, with a period length of 6 mm (about 1/8 of the 4 GHz EM wave wavelength), impedance can change from  $-500j$  to  $-10j$  at 4GHz by adjusting variables like  $a, b, w, L$ , and  $N$ . Therefore, the goal of optimizing the metal layer impedance function

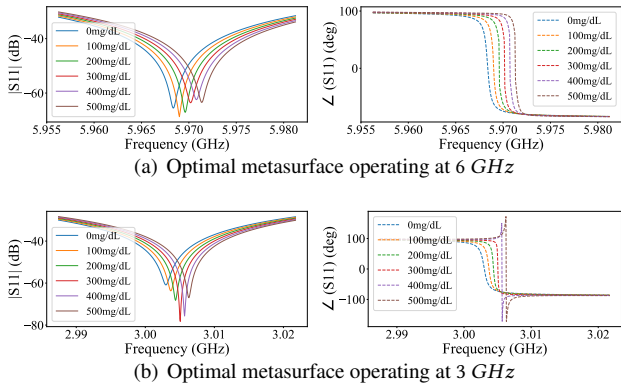


**Figure 9: Frequency response of the glucose solution (3 mm of thickness) with different concentration based on the optimized metasurface design**

is to optimize each layer's geometric parameters, namely,  $L$ ,  $a$ ,  $b$ ,  $w$ , and  $N$ . To facilitate fabrication, we let each layer's metasurface unit share  $L$ . Our optimization goal becomes finding the optimal geometric parameters of the metasurface unit, ensuring that  $X(f; L, a, b, w, N)$  maximizes sensitivity to glucose concentration changes.

Consequently, it is essential to obtain the metal pattern's impedance function for various geometric parameters and establish a relationship between these parameters and the impedance function coefficients. Fig.8 shows the impedance (imaginary part) for the 1-6 GHz frequency range under different geometric parameter patterns, obtained using HFSS. The curves can be approximated by an n-order polynomial function, i.e.,  $X(f) = X_1 f^n + X_2 f^{n-1} + \dots + X_{n+1}$ . For each  $X_i$  coefficient, an equation incorporating geometric parameters is fitted, i.e.,  $X_i = F_i(L, a, w, b, N)$ . This way, impedance information with respect to frequency can be directly obtained based on geometric parameters, enabling optimal geometric parameter determination to maximize metasurface sensitivity to liquid concentration. By modeling the impedance function concerning the metal pattern's geometric parameters, we can determine the optimal metasurface design for each layer. This is done by optimizing the objective equation and using a gradient descent optimizer to maximize  $S_{11}$  parameter sensitivity to glucose concentration. The optimization objective function can also be written as follows:

$$\max_{S_1(f), \dots, S_k(f)} \sum_{i=1}^m \sum_{j=1, j \neq i}^m \|S_{11}(c_i) - S_{11}(c_j)\|^2 \quad (8)$$

where  $S_1(f), \dots, S_k(f)$  represent the geometric parameters of the  $k$  metal layers, i.e.,  $a, w, b, N$ . Additionally, hyperparameters like the shared period length  $L$  of each metasurface unit, the number of metal and substrate layers, can be adjusted using hyperparameter tuning techniques, such as NNI [36], to obtain the most effective metasurface design within a specific frequency range.

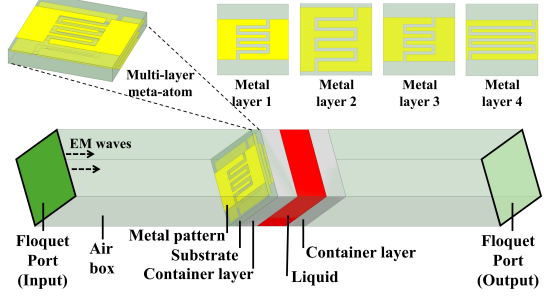


**Figure 10: HFSS simulation model of the proposed multi-layer metasurface based liquid sensing**

We present two optimized metasurface designs for sensing the glucose solution with water as the background using the equivalent circuit optimization method. One operates within the frequency range of 5.9-6.1 GHz, and the other at 2.9-3.1 GHz. Fig.9 shows the corresponding  $S_{11}$  parameters for varying glucose solution concentrations. Fig.9(a) represents the optimized metasurface resonating around 6 GHz with  $L=6$  mm, featuring 4 metal and 4 substrate layers. Glucose concentration changes cause a resonance point shift, with a frequency shift of approximately 0.8 MHz per 100 mg/dL. Although small, the  $S_{11}$  amplitude parameters for each concentration are well differentiated. At a resonance frequency of 0 mg/dL, increasing concentration changes the  $S_{11}$  amplitude for other concentrations at this frequency point by 5 dB per 100 mg/dL on average, and phase parameters change by nearly 50°. This difference is larger than the change in  $S_{11}$  parameters without the metasurface. Fig.9(b) demonstrates that our approach can effectively optimize the metasurface design operating around 3 GHz.

**Fine-tuning for Coupling Compensation Between Metal Layers.** Equivalent circuit models can effectively represent the impedance of each component and simulate the frequency response of the EM waves reflected by the metasurface and glucose solution using the ABCD matrix. However, accurately modeling the coupling between multiple metal layers in the metasurface is challenging, especially when the substrate layer thickness is small and the coupling is non-negligible. We validate the optimized metasurface design (as shown in Fig.9(a)) using the equivalent circuit model in HFSS software, with simulation results in Fig.11(a). The HFSS simulation results show a smooth  $S_{11}$  curve for the metasurface and liquid, with nearly constant resonance points across different concentrations. This outcome is due to ignoring the near-field coupling between the metal layers.

To compensate for the coupling effect, we use the HFSS simulator, which includes a finite element method solver to simulate EM behavior such as near-field coupling, on top of the existing optimized metasurface design and apply the same optimization objective (Eq.8) for fine-tuning. The HFSS simulation model is shown in Fig.10. We again use gradient

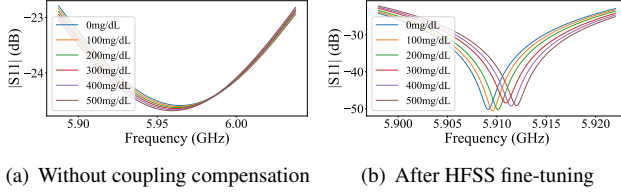


**Figure 11: Coupling compensation between multiple layers of the metasurface**

descent as the optimizer. The  $S_{11}$  parameters of the optimized metasurface design for different glucose solution concentrations are shown in Fig. 11. The results show that the metasurface design, after fine-tuning using the HFSS simulator, achieves good resonance and its resonance point shifts with the glucose solution concentration.

Although it is possible to directly use the HFSS simulation model and optimizer to optimize the metasurface for glucose solution, this approach has the following drawbacks: 1) Although HFSS finite element simulation can provide reliable EM field simulation results, the calculations are time-consuming. 2) For hyperparameter tuning, adjusting the number of metal layers, for example, requires re-establishing the HFSS simulation model, which reduces optimization efficiency. Therefore, we first establish an equivalent circuit model using the ABCD transmission matrix theory to get a rough metasurface design. We then use the HFSS simulator to compensate for the near-field coupling between the metal layers and ultimately achieve an optimized, reliable, and glucose concentration-sensitive metasurface.

## 4 EVALUATION

### 4.1 Prototype Implementation

**Metasurface fabrication.** Our optimized metasurface can be fabricated using affordable thermal printing technologies, as shown in Fig. 12. The steps include: 1) Printing metal patterns on A4 paper with a laser printer. 2) Stamping A4 paper and aluminum foil with a laminator, causing toner to adhere to aluminum powder and form a metallic layer pattern. 3) Using a PVC board as the substrate layer and assembling A4 papers with metal patterns and PVC boards to construct the final multilayer metasurface.

We test the feasibility of our system using different containers. Fig. 13 displays various sizes and types of containers. Fig. 13(a)-(c) show square containers made of Acrylics boards, with 2 mm thick PMMA material for the walls and 3 mm thick PMMA for the cavity (*i.e.*, the liquid's thickness). Fig. 13(d) presents a bionic blood vessel used as a vessel, featuring a 3 mm inner diameter and 2 mm thick silicone material for the wall thickness. To construct an equivalent circuit, we set the substrate layer to be composed of A4 paper and PVC board together, where the transmission line length

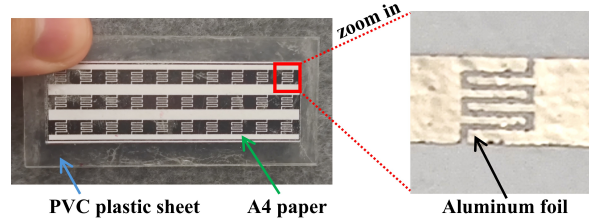


**Figure 12: An example of the fabricated metasurface**

of A4 paper is 0.1 mm, with permittivity of  $2.3 - 0.01j$ , and the transmission line length of PVC board is 0.3 mm, its permittivity is  $2.7 - 0.02j$ . For the container layers, we set the transmission line of PMMA to 2 mm, with permittivity of  $2.7 - 0.02j$ , and the transmission line of silicone material to 2 mm, with permittivity of  $2.5 - 0.02j$ .

**Testing liquid and metasurface parameters.** We create glucose solutions of varying concentrations using water and  $C_6H_{12}O_6$  powder with ground truth. We set the permittivity parameters of the glucose solution at different concentrations using models in Fig. 2. We fabricate the metasurface for the glucose with water as background. After attached to glucose solutions, the optimized metasurface demonstrates an operational frequency of 5.9 GHz. The following presents the detailed geometric parameters of the metal layers within the metasurface:

Parameters	Layer1	Layer2	Layer3	Layer4
a (mm)	2.2562	3.0091	2.1601	5.5051
b (mm)	3.4167	5.3572	3.6616	3.3134
w (mm)	0.2433	0.2666	0.3160	0.2489
N	6	6	6	6

**Table 2: Optimized parameters of the metasurface for glucose solutions with water background, and L = 6 mm**

**Experiment Setup.** We use a vector network analyzer (VNA), *i.e.*, Keysight E5071C, to measure  $S_{11}$  parameters, and alternative devices, such as a USRP, could be employed to perform the same function. Two directional UWB antennas (operating frequency range 1.5-9 GHz) are used for measurement, with one as transmitting antenna (Tx) and the other as receiving antenna (Rx), assessing metasurface-based liquid concentration sensing using the VNA. The experimental setup is shown in Fig. 13. We ensure the Tx and Rx antennas' positions allow the emitted beam to be picked up by the Rx antenna after interacting with the metasurface or liquid, and the Tx antenna emits the EM wave at a minimal oblique incidence angle to ensure the metasurface's performance. From the bottom of Fig. 13, we observe that the  $S_{11}$  curve does not exhibit any resonance in the 3-8 GHz range when there is only liquid, and similarly, the  $S_{11}$  curve does not show resonance either when there is only a metasurface. Resonance occurs only when the metasurface and target liquid are combined, confirming the initial feasibility of our optimized metasurface.

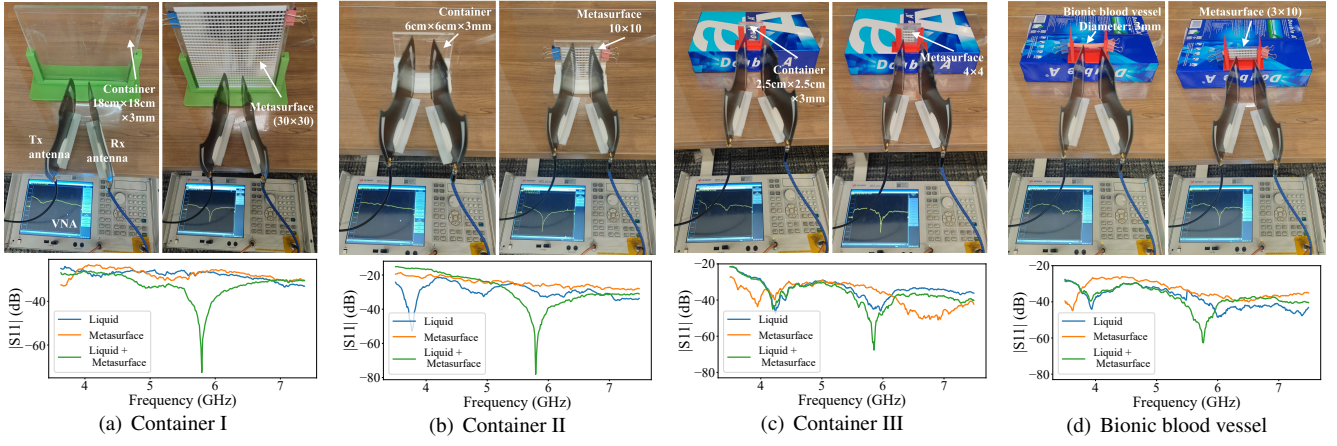


**Figure 13:** Top: Four experimental setups with different sizes (or type) of containers and metasurfaces. Bottom:  $S_{11}$  parameters of liquid alone, metasurface alone, and metasurface combined with liquid

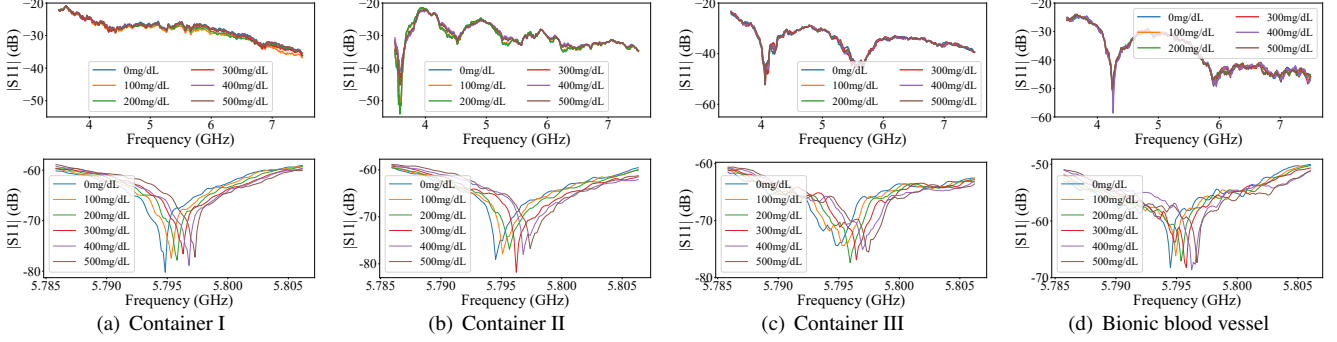


**Figure 14:** Measured  $S_{11}$  parameters of glucose solutions (with water background) at varying concentrations. Top subfigures represent  $S_{11}$  curves without metasurfaces, while bottom depict  $S_{11}$  curves with the optimized metasurfaces

## 4.2 Optimized Metasurface-based Glucose Level Monitoring Performance

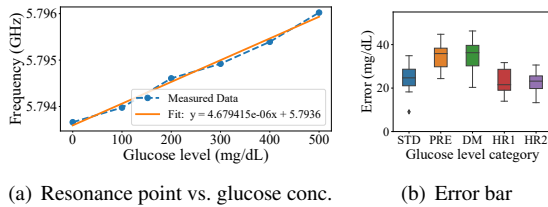
**4.2.1 Effectiveness of the optimized metasurface.** We measure  $S_{11}$  curves for various glucose solutions at different concentrations using four experimental setups with metasurfaces matching container and vessel surface areas. Fig. 14 shows the  $S_{11}$  curves with and without metasurfaces. We observe that determining glucose concentration solely based on EM wave reflection is not feasible, and  $S_{11}$  curves are susceptible to environmental multipath. In an 18 cm  $\times$  18 cm container, the multipath effect is minimal, resulting in a flat  $S_{11}$  curve. However, in smaller containers and biomimetic blood vessels,  $S_{11}$  curves show unevenness due to multipath effects. Upon adding the optimized metasurface, the  $S_{11}$  curve exhibits prominent resonance around 5.9 GHz, and the resonance point shifts right as glucose concentration increases.

We observe a minor discrepancy between the resonance points of the testbed results ( $\sim$ 5.8 GHz) and the HFSS simulation results ( $\sim$ 5.9 GHz). Although the HFSS simulation results are relatively accurate, a small gap remains likely

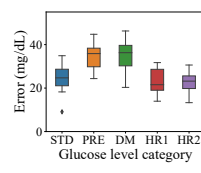
because there are some small differences between the permittivity values used in the simulation versus their values in the real-world experiments. The resonance point difference is within 0.1 GHz, which is acceptable. Moreover, the EM wave generated by our Tx antenna is incident obliquely (e.g., incident angle of 5°) to the metasurface, which further contributes to a slight variation in the resonance point.

It should be noted that the resonance generated by our metasurface and glucose solutions is not due to environmental multipath cancellation nulls or the metasurface's inherent resonance. As shown in Fig. 13, the metasurface is closely attached to the liquid container and does not alter environmental multipath. By comparing  $S_{11}$  curves with and without the metasurface, we observe that resonance occurs only after coupled with the liquid, exhibiting robustness against multipath and compatibility with various container setups.

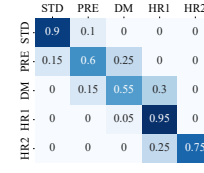
**4.2.2 Glucose Level Identification.** We fit the relationship between resonance points and glucose concentrations, as changes in concentration affect  $S_{11}$  resonance points. Testing resonance point information in a bionic blood vessel (Fig. 13(d)) across six cases (0-500 mg/dL), we find a linear



(a) Resonance point vs. glucose conc.

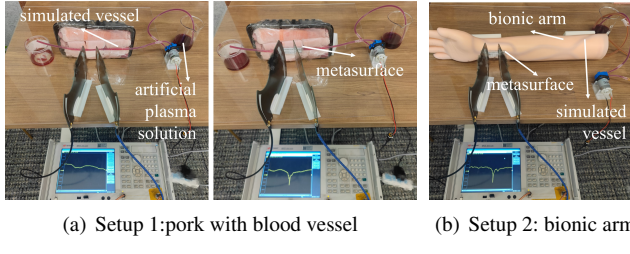


(b) Error bar



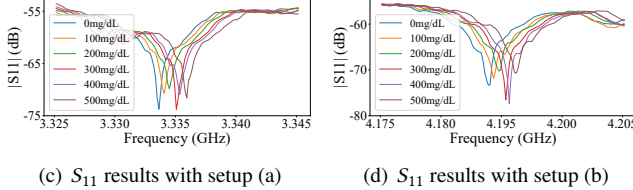
(c) Confusion matrix

**Figure 15: Analyzing predicted glucose values using the fit model in various regions: STD (<120 mg/dL), PRE (120-180 mg/dL), DM (180-240 mg/dL), HR1 (240-400 mg/dL), HR2 (>400 mg/dL)**



(a) Setup 1:pork with blood vessel

(b) Setup 2: bionic arm

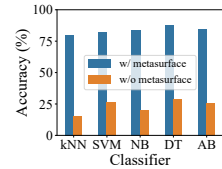

 (c)  $S_{11}$  results with setup (a)

 (d)  $S_{11}$  results with setup (b)

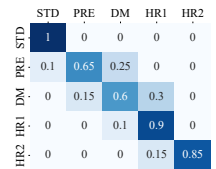
**Figure 17: Glucose monitoring experiment setups and measured  $S_{11}$  values for artificial plasma glucose solutions at varying concentrations**

proportional relationship (Fig. 15(a)), enabling direct glucose concentration inference from resonance points.

To evaluate glucose concentration detection accuracy, we prepare solutions at 20 mg intervals (0-500 mg/dL) and test each concentration four times to obtain  $S_{11}$  curves and resonance points. Based on the results in Fig. 15(a), we can infer glucose concentrations and obtain the results. We categorize the glucose level range into five regions, and report identification errors in Fig. 15(b), respectively. The optimized metasurface maintains average errors of 28 mg/dL. Note that ISO 15197:2013 (15%) range [25] Our system achieve average error rate ranging from -13.23% to 11.86%, i.e.,  $\frac{\text{error}}{\text{groundtruth}}$ , for blood glucose monitoring, within the ISO 15197:2013 ( $\pm 15\%$ ) range [25], which is an international standard for diabetes management. We also apply commonly used classification models to categorize glucose concentration levels. Selecting the  $S_{11}$  parameters at 5.5-6.5 GHz, we collect data from 0-500 mg/dL with and without metasurface at 20 mg/dL intervals. The classification results are depicted in Fig. 16(a), where NB means Naive Bayes, DT means Decision Tree, and AB means AdaBoost. We observe that using entire  $S_{11}$  curves after using metasurface (instead of just resonant points)

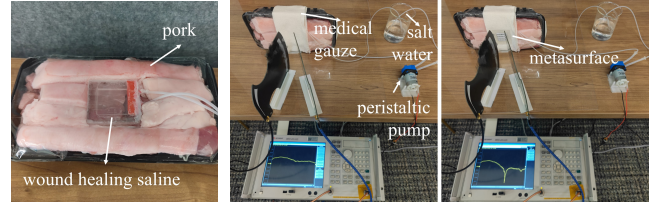


(a) Performances of five common classifiers



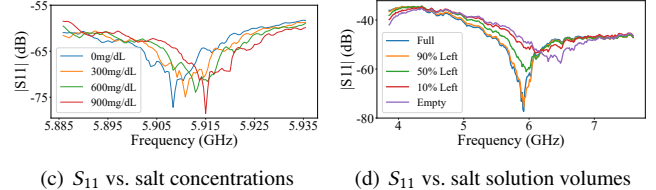
(b) Confusion matrix of DT

**Figure 16: Classification performance of the glucose levels (5 categories) with and without metasurface**



(a) Simulated wound

(b) Setup: saline in gauze for healing wounds


 (c)  $S_{11}$  vs. salt concentrations

 (d)  $S_{11}$  vs. salt solution volumes

**Figure 18: Wound recovery monitoring experiment setups and measured  $S_{11}$  values for NaCl solutions at varying concentrations with water background**

Parameters	Layer1	Layer2	Layer3	Layer4
a (mm)	4.2331	3.0312	5.2703	3.6779
b (mm)	2.9597	4.0970	4.2225	2.0468
w (mm)	0.2324	0.2094	0.2867	0.2812
N	6	6	6	6

**Table 3: Optimized parameters of the metasurface for glucose solutions with artificial plasma background**

provide more information about liquid concentration. The accuracy of classification using the DT model reaches 81%, with the corresponding confusion matrix displayed in Fig. 16(b).

### 4.3 Applications

**4.3.1 Blood glucose monitoring.** We use pork and blood vessels, along with a bionic arm, to simulate the experimental scenario of a human body as closely as possible. The experimental setups are depicted in Fig. 17. We inject glucose into artificial plasma, resembling human blood[48]. Utilizing permittivity data from [54], we fit the Cole-Cole model over the UWB frequency. We develop a metasurface specifically for artificial plasma as the glucose solution, which operates at 3.3 GHz when attached. The detailed geometric parameters of the metal layers are provided in Table 3, and the shared parameter  $L=6$  mm. The experimental results, also shown in

Fig. 17, demonstrate that our optimized metasurface can also couple with plasma in blood vessels and achieve resonance point shifts in response to changes in glucose concentration. We also employed a linear fit to establish the relationship between the resonance point and glucose concentration in the setup 2 in Fig. 17. The experiments result in a glucose concentration error of 32 mg/dL and a 78% accuracy in classifying the five glucose regions (the same regions as Fig. 15).

**4.3.2 Wound recovery monitoring.** Besides glucose level identification, we test our metasurface in detecting different substance concentrations. In medicine, saline is added to gauze to accelerate wound healing [5]. However, gauze opacity prevents physicians from accurately assessing saline absorption and wound recovery. Furthermore, it is crucial to determine when to replace the gauze to replenish the saline healing solution. We apply the proposed MetaPatch to solve the above two problems, and create saline solutions using pure water and NaCl powder for detecting saline concentrations. First, we use permittivity data from[39] to fit the Cole-Cole model over the UWB frequency and fabricate a metasurface specifically for saline solutions. With the metasurface attached, the operational frequency is 6 GHz, and the metal layer geometric parameters are in Table 4, and the shared parameter  $L=6$  mm. We set up a wound-healing scenario as shown in Fig. 18. We apply a healing solution (with a saline concentration of about 900 mg/dL) to a wound, which dilutes the salt concentration. The corresponding  $S_{11}$  results are in Fig. 18, and the quantitative analysis error is 24 mg/dL. Our optimized metasurface is sensitive to saline, and can be used to track salt concentration in real-time underneath gauze, allowing physicians to monitor wound healing progress. We simulate healing saline absorption into the wound by pumping NaCl solutions from the container. As shown in Fig. 18(d), significant  $S_{11}$  changes with varying volumes, and these change can help physicians decide when to change the gauze.

Parameters	Layer1	Layer2	Layer3	Layer4
a (mm)	3.4119	3.1812	5.2313	2.1142
b (mm)	3.4489	3.3860	4.5249	4.4268
w (mm)	0.2021	0.2318	0.1638	0.1849
N	6	6	6	6

**Table 4: Optimized parameters of the metasurface for saline solutions with water background**

## 5 DISCUSSION

**Effect of other components on the blood permittivity.** Permittivity, a macroscopic quantity assessing dielectric properties of liquids, contrasts with optical spectral-based glucose sensing methods [47], which focus on glucose molecule absorption spectra. Permittivity may be affected by variations in other blood components' concentrations. For example, in diabetic patients, blood glucose concentrations can range from

30 mg/dL to 400 mg/dL. In comparison, sodium and chloride levels, despite being present in significant amounts, exhibit variations between 310 mg/dL and 333 mg/dL, and 337 mg/dL and 372 mg/dL, respectively [34]. Furthermore, other minerals are found in relatively low concentrations in blood, such as magnesium (1.8-3.4 mg/dL), calcium (8.5-10.5 mg/dL), and potassium (13.6-21.4 mg/dL) [34]. Blood permittivity variations are mainly attributed to glucose concentration fluctuations [9]. Thus, we assume changes in other components' concentrations minimally impact blood permittivity, a common assumption in related studies [9, 54, 56].

**Pre-calibration for absolute glucose concentration.** Although the metasurface is effectively designed, the absolute value of the resonance point may change due to various factors when the resonance is generated by coupling the metasurface and liquid. For example, the Tx antenna's position can cause changes, as the incident angle of the EM wave on the metasurface slightly affects the metal layer's equivalent impedance. Changes in the vessel's thickness can also alter the resonance point, due to the equivalent capacitor changes. However, by maintaining consistent positions for the Tx and Rx antennas and blood vessels, we can determine relative glucose concentration changes based on resonance point offset. Our method is robust within an  $10^\circ$  angle change with the HFSS simulation results, and distance changes have minimal impact on estimation accuracy due to the stable frequency response across distances. Notably, all non-invasive blood glucose measurement methods require initial precise calibration for accurate absolute blood glucose level measurements. A common calibration approach combines non-invasive methods with invasive techniques, fine-tuning non-invasive methods based on invasive measurements for reliable blood glucose monitoring. This suggests our approach holds promise for practical use.

## 6 CONCLUSION

In this paper, we develop a metasurface based contactless system for sensing the concentration changes of components in a liquid, *e.g.*, glucose or salt concentration. Our system is built on a solid theoretical foundation by modeling the metasurface's coupling with the liquid under different concentrations using an equivalent circuit and deriving the metasurface impedance that maximizes the difference in the reflection coefficients corresponding to different concentrations. We fabricate our metasurface at close to 0 cost. Our experimental results show the system yields good accuracy. We present the first design of using metasurface to sense thin liquid. A lot need to be done before it can be deployed, including enhancing its accuracy and robustness as well as conducting user studies. We hope our work could inspire other researchers to further explore its potential and ultimately realize robust noninvasive glucose sensing to benefit millions of patients.

## REFERENCES

- [1] J. A. Al-Lawati. Diabetes mellitus: a local and global public health emergency! *Oman medical journal*, 32(3):177, 2017.
- [2] Ansys. Ansys hfss best-in-class 3d high frequency structure simulation software. <https://www.ansys.com/zh-cn/products/electronics/ansys-hfss>, 2023.
- [3] I. J. Bahl and P. Bhartia. Microwave solid state circuit design. *Wiley Interscience*, 2003.
- [4] A. Bauer, O. Hertzberg, A. Küderle, D. Strobel, M. A. Pleitez, and W. Mäntele. Ir-spectroscopy of skin in vivo: Optimal skin sites and properties for non-invasive glucose measurement by photoacoustic and photothermal spectroscopy. *Journal of biophotonics*, 11(1):e201600261, 2018.
- [5] K. Breuing, E. Eriksson, P. Liu, and D. R. Miller. Healing of partial thickness porcine skin wounds in a liquid environment. *Journal of Surgical Research*, 52(1):50–58, 1992.
- [6] M. R. Burge, S. Mitchell, A. Sawyer, and D. S. Schade. Continuous glucose monitoring: the future of diabetes management. *Diabetes Spectrum*, 21(2):112–119, 2008.
- [7] N. Campus. Noviosense. <https://noviosense.com/>, 2023.
- [8] G. Cappon, M. Vettoretti, G. Sparacino, and A. Facchinetto. Continuous glucose monitoring sensors for diabetes management: a review of technologies and applications. *Diabetes & metabolism journal*, 43(4):383–397, 2019.
- [9] E. L. Chuma, Y. Iano, G. Fontgalland, and L. L. B. Roger. Microwave sensor for liquid dielectric characterization based on metamaterial complementary split ring resonator. *IEEE Sensors Journal*, 18(24):9978–9983, 2018.
- [10] Cnoga. Cog hybrid glucometer. <https://www.cnogacare.co/cog-hybrid-glucometer>, 2023.
- [11] CONGA. Cog - hybrid glucometer: Meet the world's first hybrid, non-invasive glucometer. <https://www.cnogacare.co/cog-hybrid-glucometer>, 2023.
- [12] Danatach. Weighing cgm pros and cons. [https://www.diabeteseducator.org/danatech/glucose-monitoring/continuous-glucose-monitors-\(cgm\)/cgm-101/pros-cons-of-cgm](https://www.diabeteseducator.org/danatech/glucose-monitoring/continuous-glucose-monitors-(cgm)/cgm-101/pros-cons-of-cgm), 2023.
- [13] A. Dhekne, M. Gowda, Y. Zhao, H. Hassanieh, and R. R. Choudhury. Liquid: A wireless liquid identifier. In *Proceedings of the 16th annual international conference on mobile systems, applications, and services*, pages 442–454, 2018.
- [14] A. Ebrahimi, J. Scott, and K. Ghorbani. Microwave reflective biosensor for glucose level detection in aqueous solutions. *Sensors and Actuators A: Physical*, 301:111662, 2020.
- [15] C. Feng, J. Xiong, L. Chang, J. Wang, X. Chen, D. Fang, and Z. Tang. Wimi: Target material identification with commodity wi-fi devices. In *2019 IEEE 39th International Conference on Distributed Computing Systems (ICDCS)*, pages 700–710. IEEE, 2019.
- [16] P. Geelhoed-Duijvestijn, D. Vegelyte, A. Kownacka, N. Anton, M. Joosse, and C. Wilson. Performance of the prototype noviosense noninvasive biosensor for tear glucose in type 1 diabetes. *Journal of Diabetes Science and Technology*, 15(6):1320–1325, 2021.
- [17] S. Guin and M. Chattopadhyay. Advancement and challenges for non-invasive monitoring of blood glucose: a review. *Advances in Medical Physics and Healthcare Engineering: Proceedings of AMPHE 2020*, pages 101–113, 2021.
- [18] R. Gulich, M. Köhler, P. Lunkenheimer, and A. Loidl. Dielectric spectroscopy on aqueous electrolytic solutions. *Radiation and environmental biophysics*, 48:107–114, 2009.
- [19] U. Ha, J. Leng, A. Khaddaj, and F. Adib. Food and liquid sensing in practical environments using rfids. In *Proceedings of the 17th USENIX Symposium on Networked Systems Design and Implementation (NSDI'20)*, 2020.
- [20] U. Ha, Y. Ma, Z. Zhong, T.-M. Hsu, and F. Adib. Learning food quality and safety from wireless stickers. In *Proceedings of the 17th ACM workshop on hot topics in networks*, pages 106–112, 2018.
- [21] J. Hanna, Y. Tawk, S. Azar, A. H. Ramadan, B. Dia, E. Shamieh, S. Zoghbi, R. Kanj, J. Costantine, and A. A. Eid. Wearable flexible body matched electromagnetic sensors for personalized non-invasive glucose monitoring. *Scientific Reports*, 12(1):14885, 2022.
- [22] T. Harris. Best glucose meters to monitor your blood sugar in 2023. <https://www.forbes.com/health/conditions/diabetes/best-glucose-meters/>, 2023.
- [23] J. Huang, Y. Zhang, and J. Wu. Review of non-invasive continuous glucose monitoring based on impedance spectroscopy. *Sensors and Actuators A: Physical*, 311:112103, 2020.
- [24] X. Huang, C. Leduc, Y. Ravussin, S. Li, E. Davis, B. Song, Q. Wang, D. Accili, R. Leibel, and Q. Lin. Continuous monitoring of glucose in subcutaneous tissue using microfabricated differential affinity sensors. *Journal of diabetes science and technology*, 6(6):1436–1444, 2012.
- [25] ISO. Iso 15197:2013 in vitro diagnostic test systems requirements for blood-glucose monitoring systems for self-testing in managing diabetes mellitus. <https://www.iso.org/standard/54976.html>, 2023.
- [26] ISRAEL21C. Test your glucose level without drawing blood. <https://www.israel21c.org/test-your-glucose-level-without-drawing-blood/>, 2023.
- [27] J. W. Kang, Y. S. Park, H. Chang, W. Lee, S. P. Singh, W. Choi, L. H. Galindo, R. R. Dasari, S. H. Nam, J. Park, et al. Direct observation of glucose fingerprint using in vivo raman spectroscopy. *Science Advances*, 6(4):eaay5206, 2020.
- [28] T. Karacolak, E. C. Moreland, and E. Topsakal. Cole-cole model for glucose-dependent dielectric properties of blood plasma for continuous glucose monitoring. *Microwave and Optical Technology Letters*, 55(5):1160–1164, 2013.
- [29] L. Kennedy. Finger-stick glucose monitoring. <https://www.ncbi.nlm.nih.gov/pmc/articles/PMC2845057/>, 2023.
- [30] S. Kim, J. Malik, J. M. Seo, Y. M. Cho, and F. Bien. Subcutaneously implantable electromagnetic biosensor system for continuous glucose monitoring. *Scientific Reports*, 12(1):17395, 2022.
- [31] Labmedica. Noninvasive device monitors people with diabetes. <https://www.labmedica.com/clinical-chemistry/articles/294759904/noninvasive-device-monitors-people-with-diabetes.html>, 2023.
- [32] LDTDesign. Medical and healthcare non-invasive blood glucose monitor. <https://www.ltddesign.co.uk/our-work/non-invasive-blood-glucose-monitor/>, 2023.
- [33] Y. Liang, A. Zhou, H. Zhang, X. Wen, and H. Ma. Fg-liquid: A contactless fine-grained liquid identifier by pushing the limits of millimeter-wave sensing. *Proceedings of the ACM on Interactive, Mobile, Wearable and Ubiquitous Technologies*, 5(3):1–27, 2021.
- [34] T. H. S. Library. University of michigan library. <https://www.lib.umich.edu/locations-and-hours/taubman-health-sciences-library>, 2023.
- [35] H. A. MacKenzie, H. S. Ashton, S. Spiers, Y. Shen, S. S. Freeborn, J. Hannigan, J. Lindberg, and P. Rae. Advances in photoacoustic noninvasive glucose testing. *Clinical chemistry*, 45(9):1587–1595, 1999.
- [36] Microsoft. An open source automl toolkit for automate machine learning lifecycle. <https://github.com/microsoft/nni>, 2023.
- [37] E. Moser, L. Crew, and S. Garg. Role of continuous glucose monitoring in diabetes management. *Avances en Diabetología*, 26(2):73–78, 2010.
- [38] H. news. Non-invasive device could end daily finger pricking for people with diabetes. [https://www.leeds.ac.uk/news/article/3723/non-invasive\\_device\\_could\\_end\\_daily\\_finger\\_pricking\\_for\\_people\\_with\\_diabetes](https://www.leeds.ac.uk/news/article/3723/non-invasive_device_could_end_daily_finger_pricking_for_people_with_diabetes), 2023.
- [39] K. Nörtemann, J. Hilland, and U. Kaatze. Dielectric properties of aqueous nacl solutions at microwave frequencies. *The Journal of*

- Physical Chemistry A*, 101(37):6864–6869, 1997.
- [40] N. I. of Diabetes, Digestive, and K. Diseases. Continuous glucose monitoring. <https://www.niddk.nih.gov/health-information/diabetes/overview/managing-diabetes/continuous-glucose-monitoring>, 2023.
  - [41] L. Olansky and L. Kennedy. Finger-stick glucose monitoring: issues of accuracy and specificity, 2010.
  - [42] A. E. Omer, S. Safavi-Naeini, R. Hughson, and G. Shaker. Blood glucose level monitoring using an fmcw millimeter-wave radar sensor. *Remote Sensing*, 12(3):385, 2020.
  - [43] A. E. Omer, G. Shaker, S. Safavi-Naeini, H. Kokabi, G. Alquié, F. Deshours, and R. M. Shubair. Low-cost portable microwave sensor for non-invasive monitoring of blood glucose level: Novel design utilizing a four-cell csrr hexagonal configuration. *Scientific Reports*, 10(1):15200, 2020.
  - [44] M. A. Pleitez, T. Lieblein, A. Bauer, O. Hertzberg, H. von Lilienfeld-Toal, and W. Mantele. In vivo noninvasive monitoring of glucose concentration in human epidermis by mid-infrared pulsed photoacoustic spectroscopy. *Analytical chemistry*, 85(2):1013–1020, 2013.
  - [45] D. M. Pozar. *Microwave engineering*. John wiley & sons, 2011.
  - [46] D. M. Pozar. *Microwave Engineering (4th Edition)*. John Wiley & Sons, Inc., 2011.
  - [47] P. S. K. Reddy, D. Mahesh, C. U. Teja, M. Janaki, and K. Mannem. Non-invasive glucose monitoring using nir spectroscopy. In *Journal of Physics: Conference Series*, volume 2325, page 012021. IOP Publishing, 2022.
  - [48] S. Sarkar. Artificial blood. <https://www.ncbi.nlm.nih.gov/pmc/articles/PMC2738310/>, 2023.
  - [49] G. Shaker, K. Smith, A. E. Omer, S. Liu, C. Csech, U. Wadhwa, S. Safavi-Naeini, and R. Hughson. Non-invasive monitoring of glucose level changes utilizing a mm-wave radar system. *International Journal of Mobile Human Computer Interaction (IJMHCI)*, 10(3):10–29, 2018.
  - [50] C. Shan, H. Yang, J. Song, D. Han, A. Ivaska, and L. Niu. Direct electrochemistry of glucose oxidase and biosensing for glucose based on graphene. *Analytical chemistry*, 81(6):2378–2382, 2009.
  - [51] F. Shang, P. Yang, Y. Yan, and X.-Y. Li. Liqray: non-invasive and fine-grained liquid recognition system. In *Proceedings of the 28th Annual International Conference on Mobile Computing And Networking*, pages 296–309, 2022.
  - [52] J. Y. Sim, C.-G. Ahn, E.-J. Jeong, and B. K. Kim. In vivo microscopic photoacoustic spectroscopy for non-invasive glucose monitoring invulnerable to skin secretion products. *Scientific reports*, 8(1):1059, 2018.
  - [53] C. Song, W.-H. Fan, L. Ding, X. Chen, Z.-Y. Chen, and K. Wang. Terahertz and infrared characteristic absorption spectra of aqueous glucose and fructose solutions. *Scientific Reports*, 8(1):8964, 2018.
  - [54] E. Topsakal, T. Karacolak, and E. C. Moreland. Glucose-dependent dielectric properties of blood plasma. In *2011 XXXth URSI General assembly and scientific symposium*, pages 1–4. IEEE, 2011.
  - [55] T. Torii, H. Chiba, T. Tanabe, and Y. Oyama. Measurements of glucose concentration in aqueous solutions using reflected thz radiation for applications to a novel sub-thz radiation non-invasive blood sugar measurement method. *Digital health*, 3:2055207617729534, 2017.
  - [56] V. Turgul and I. Kale. Characterization of the complex permittivity of glucose/water solutions for noninvasive rf/microwave blood glucose sensing. In *2016 IEEE International Instrumentation and Measurement Technology Conference Proceedings*, pages 1–5. IEEE, 2016.
  - [57] Wikipedia. Permittivity. <https://en.wikipedia.org/wiki/Permittivity>, 2023.
  - [58] B. Xie, J. Xiong, X. Chen, E. Chai, L. Li, Z. Tang, and D. Fang. Tagtag: material sensing with commodity rfid. In *Proceedings of the 17th conference on embedded networked sensor systems*, pages 338–350, 2019.
  - [59] J. Yadav, A. Rani, V. Singh, and B. M. Murari. Prospects and limitations of non-invasive blood glucose monitoring using near-infrared spectroscopy. *Biomedical signal processing and control*, 18:214–227, 2015.
  - [60] J. Yang, L. Qi, B. Li, L. Wu, D. Shi, J. A. Uqaili, and X. Tao. A terahertz metamaterial sensor used for distinguishing glucose concentration. *Results in Physics*, 26:104332, 2021.